Impact of tumor and epithelial phenotypes on metabolism in breast cancer

Heather Ann Brauer[1], **Liza Makowski**[2,3], **Katherine A. Hoadley**[3], **Patricia Casbas-Hernandez**[4], **Lindsay J. Lang**[1], **Erick Romàn-Pèrez**[1], **Monica D'Arcy**[1], **Alex J. Freemerman**[2], **Charles M. Perou**[3,4,5], and **Melissa A. Troester**[1,3,4]

[1]Department of Epidemiology, Gillings School of Global Public Health, University of North Carolina at Chapel Hill, Chapel Hill, NC 27599

[2]Department of Nutrition, Gillings School of Global Public Health, University of North Carolina at Chapel Hill, Chapel Hill, NC 27599

[3]Lineberger Comprehensive Cancer Center, University of North Carolina at Chapel Hill, Chapel Hill, NC 27599

[4]Department of Pathology and Laboratory Medicine, School of Medicine, University of North Carolina at Chapel Hill, Chapel Hill, NC 27599

[5]Department of Genetics, School of Medicine, University of North Carolina at Chapel Hill, Chapel Hill, NC 27599

Abstract

Purpose—Cancer cells have altered metabolism, with increased glucose uptake, glycolysis, and biomass production. This study performed genomic and metabolomic analyses to elucidate how tumor and stromal genomic characteristics influence tumor metabolism.

Experimental Design—Thirty-three breast tumors and six normal breast tissues were analyzed by gene expression microarray and by mass spectrometry for metabolites. Gene expression data and clinical characteristics were evaluated in association with metabolic phenotype. To evaluate the role of stromal interactions in altered metabolism, cocultures were performed using breast cancer cells and primary cancer-associated fibroblasts (CAFs).

Results—Across all metabolites, unsupervised clustering resulted in two main sample clusters. Normal breast tissue and a subset of tumors with less aggressive clinical characteristics had lower levels of nucleic and amino acids and glycolysis byproducts, while more aggressive tumors had higher levels of these Warburg-associated metabolites. While tumor intrinsic subtype did not predict metabolic phenotype, metabolic cluster was significantly associated with expression of a wound response signature. In cocultures, CAFs from basal-like breast cancers increased glucose up take and basal-like epithelial cells increased glucose oxidation and glycogen synthesis, suggesting interplay of stromal and epithelial phenotypes on metabolism. Cytokine arrays identified hepatocyte growth factor (HGF) as a potential mediator of stromal-epithelial interaction, and antibody neutralization of HGF resulted in reduced expression of glucose transporter 1 (GLUT1) and decreased glucose uptake by epithelium.

Conclusions—Both tumor/epithelial and stromal characteristics play important roles in metabolism. Warburg-like metabolism is influenced by changes in stromal-epithelial interactions, including altered expression of HGF/Met pathway and GLUT1 expression.

Correspondence to: Melissa A. Troester.

Keywords

tumor-stromal cell interactions; metabolomics; breast cancer; genomics; microenvironment

Introduction

Highly proliferative tumor cells undergo fundamental changes in metabolism and nutrient usage to survive and progress (1), and metabolic transformation appears to be necessary for sustained proliferation (2). Much of the metabolic transformation is glucose-dependent, with invasive cancers exhibiting increased aerobic glycolysis (3) via the "Warburg Effect"(4). The Warburg effect occurs when there is a metabolic shift towards glycolysis, with increased cellular production of biomass, especially amino acids and nucleic acids. While the Warburg phenomenon has been investigated for over 85 years, the metabolic interactions between stroma and epithelium are not well characterized, despite the important role of stroma in breast cancer biology (5-12).

The gap in our understanding of stromal-epithelial interactions was recently illuminated when it was shown that epithelial tumor cells induce oxidative stress in the normal stroma (9), in turn leading to activation of NFκB and HIF-1α pathways in cancer-associated fibroblasts (CAFs) (11). Concomitant changes in inflammation, autophagy, mitophagy, and aerobic glycolysis are induced in the stroma, which then produces energy-rich metabolites (such as lactate and pyruvate) that are secreted and used by epithelial cells to generate ATP (11, 13). This bidirectional communication, with aerobic glycolysis in stroma fueling cancer growth is referred to as "Reverse Warburg Effect" (14-16), and its discovery established an important role for stroma in altering metabolism (9-11). However, differences in metabolomics by stromal-epithelial interaction and according to breast cancer subtype have not been widely investigated.

Breast tumors show substantial heterogeneity (17) with at least five distinct subtypes: luminal A, luminal B, HER2-positive, basal-like, and claudin low breast cancers (18-20). In addition to their unique cell-autonomous characteristics [including unique mutation patterns, chemotherapy responses, and cellular phenotypes (21-23)], these subtypes have distinct interactions with the stroma. The interaction of basal-like breast cancer cells with fibroblasts leads to an increase in inflammatory cytokines and migratory behavior, while luminal cells in culture with fibroblasts demonstrate distinct gene expression and altered proliferation (12, 24). This evidence of subtype-specific interactions with surrounding stroma underscores the importance of studying epithelial and stromal factors simultaneously when evaluating tumor metabolism.

In the present study, we apply metabolomics and radiotracer metabolic studies to simultaneously investigate the role of tumor gene expression and stromal-epithelial interactions in tumor metabolism. Tissue samples were used to perform gene expression and samples were classified using multiple published signatures: the PAM50 signature, claudin low signature, and *in vivo* wound response signature (17, 20, 25). These gene expression phenotypes were then compared with metabolomics classes identified by analysis of 379 metabolites. Complementary coculture experiments were performed to evaluate subtype-specific metabolic interactions of stromal and epithelial cells experimentally. Our results illustrate that compared to luminal cancer cells or luminal-derived cancer associated fibroblasts (CAFs), basal-like cells and basal-like CAFs play a strong role in determining substrate metabolism in culture. Strong associations between tissue metabolic phenotype and tissue gene expression also suggest the importance of stroma in metabolic cancer microenvironments.

Methods

Patient samples

31 fresh frozen breast tumor samples, 6 breast tissue samples from reduction mammoplasty, and 5 metastatic samples were obtained under IRB-approved protocols at the University of North Carolina at Chapel Hill (UNC-CH). Patients were treated according to the standard of care dictated by disease stage, ER, and HER2 status. Table 1 describes patient demographics and tumor characteristics. All tissues were handled by snap freezing immediately after surgery, and RNA was isolated using a protocol as described by Hu et al. (26). RNA integrity was determined using the RNA 6000 Nano LabChip Kit and Agilent 2100 Bioanalyzer.

Microarrays

Microarrays experiments were performed as described (26). Briefly, labeled cRNA was generated using Agilent's Low RNA Input Linear Amplification Kit. Cy5-labeled experiment samples were combined with Cy3-labeled reference (Stratagene Universal Human Reference spiked with 1:1,000 with MCF-7 RNA and 1:1,000 with ME16C RNA to increase expression of breast cancer genes) and hybridized to 4×44K Agilent whole genome arrays or 244K Agilent custom arrays. For two cases with duplicate arrays, the intraclass correlation coefficients (ICC) were 0.597 and 0.886, suggesting moderate to strong agreement between replicates. All tumor gene expression data are publicly available through the Gene Expression Omnibus (GSE6128 and GSE6130).

Metabolite arrays

For each tumor, a single sample was analyzed for metabolites. Tissue (100 mg) was homogenized in a volume of water at 4 µL per mg of sample in a 2 mL cryovial with two 3mm Zirconium oxide beads, one 3/8 steel ballcone and one 1/8 steel ballcone on the GenoGrinder at 1000 strokes/minute for five minutes. A 100 µL aliquot of the homogenate was placed in a 96-well deepwell plate along with two 3mm Zirconium oxide grinding beads per well. The plate was placed in the chiller on the robot and a 400 µL volume of EtOAc/ EtOH (1:1) with 2.5 µg/mL 2-fluorophenylglycine and 25 µg/mL d2-maleic acid and tridecanoic acid was added to each well. The plate was capped with a plate mat and samples were shaken on GenoGrinder at 675 strokes/ minute for two minutes. The plate was centrifuged on a Beckman GS-6R centrifuge at 3200 RPM for 5 minutes at 4°C then placed back on the Hamilton LabStar robot and the centrifugates were transferred to a second plate. A 200µL volume of MeOH was placed in each well of the first plate and the plate was shaken and centrifuged as before. The centrifugates were transferred as before and the same process was repeated using 200uL volume of MeOH/H2O (3:1) and then repeated using 200uL volume of DCM/MeOH (1:1). The samples were mixed by pipetting up and down several times and a 225 µL aliquot of each was transferred to each of two 250 µL autosampler vial inserts. All extracts were placed in the Zymark Turbo Vap 96 for concentration under nitrogen streams for 25 minutes. A second 225 µL aliquot of each sample was transferred to the appropriate insert and the samples were placed in the Labconco Centrivap Concentrator for drying for 6.5 hours for drying. Samples were transferred to the Labconco Freezone 6 lyophilizer for further overnight drying. For LC/MS, a 40 µl volume of MeOH with 20 µg/mL D10-benzophenone was added to each sample. Samples were shaken with a Lab-Line Titer plate shaker for 5 minutes on setting 7 then a 60 µL volume of 0.1% formic acid was added containing 5 µg/mL d3 leucine, 5 µg/mL DL-4-chlorophenylalanine, 5 µg/mL 4-bromo-DL-phenylalanine and 0.5µg/mL amitryptyline.

For GC/MS, samples were derivatized to a final volume of 50 µl for GC/MS analysis using equal parts bistrimethyl-silyl-trifluoroacetamide and solvent mixture

acetonitrile:dichloromethane:cyclohexane (5:4:1) with 5% triethylamine at 60°C for one hour. Three types of controls were analyzed in concert with the experimental samples: samples generated from pooled experimental samples served as technical replicates throughout the data set, extracted water samples served as process blanks, and a cocktail of standards spiked into every analyzed sample allowed instrument performance monitoring. Experimental samples and controls were randomized across the platform run. Raw data is included as a supplemental table (Table S1).

Metabolite data analysis

Metabolite levels with signal intensity greater than 10 dpi in both channels and at least 80% present data were selected and the red/green Lowess normalized ratios for each gene were $\log_2$ transformed. Missing data were imputed using k-nearest neighbors' imputation (with k=10). This resulted in a complete dataset consisting of 379 metabolites and each row/metabolite was median centered. Data were analyzed by unsupervised Significance Analysis of Microarray (SAM) (27) and significant metabolites were clustered across all samples using average-linkage hierarchical cluster analysis, results were visualized using Java Treeview (28). SAM uses the variance structure of the data to compute expected distributions. Small fold changes were statistically significant by SAM analysis due to low variation between samples within a class. To test whether there was a significant trend in metabolite level for classes of metabolites [amino acids, carbohydrates/sugars, nucleic acids, and the tricarboxylic acid (TCA) cycle metabolites], we estimated the β-value and p-value corresponding to linear regression of metabolite level on an ordinal variable equal to 1 for normal tissue, 2 for Cluster 1 samples, 3 for Cluster 2 samples, and 4 for metastases. Statistical tests of the trend were two-tailed and standard error was calculated (SAS version 9.2). Because these clusters emerged from SAM analyses where multiple comparisons were adjusted, no adjustment for multiple comparisons was made in the trend analyses. The objective of these analyses is to show whether there is evidence of a monotonic increase or decrease in metabolite level.

Gene Expression Data Analysis

Using the probe set common to both array platforms (25), probes with signal intensity greater than 10 dpi in both channels and at least 80% present data were selected and the red/green Lowess normalized ratios for each gene were $\log_2$ transformed. Duplicate microarrays corresponding to the same patient sample were combined by averaging. Missing data were imputed using k-nearest neighbors' imputation (with k=10). Gene annotations from each dataset were mapped to UniGene Cluster IDs (UCIDs, Build 161) using the SOURCE database, and multiple occurrences of a UCID were collapsed by taking the median value for that ID within each experiment and platform. This resulted in a complete dataset consisting of ~2800 genes, and each experiment was standardized to N(0,1) and each row/gene was median centered.

To identify genes that significantly changed by metabolic cluster (Cluster 1 or Cluster 2) data were analyzed by two-class Significance Analysis of Microarray (27). Significant genes were clustered across all samples using average-linkage hierarchical cluster analysis and results were visualized using Java Treeview (28). Significant genes were evaluated for ontological enrichment using Ingenuity Pathway Analysis (IPA), with Benjamini–Hochberg (B-H) multiple testing correction. Significant functions and pathways were defined as those with B-H *p-values* less than 0.05.

Associations between metabolic phenotype and biologically-defined gene expression signatures

To characterize the biological phenotypes of the metabolic clusters, gene expression in each sample was compared to an existing *in vivo* breast-derived wound response signature (25). The wound response signature was generated by comparing cancer-adjacent stroma-rich breast tissue to breast tissue from reduction mammoplasty, which identified an active wound signature in the cancer-adjacent tissue. The median centered gene expression profile of each patient was evaluated for correlation with this signature by calculating Pearson correlation coefficients, using the method of Creighton *et al.* (29). Briefly, vectors corresponding to the genes in the wound response signature were constructed, with 1 assigned to up-regulated genes and -1 assigned to down-regulated genes. Sample arrays were filtered to retain only genes with interquartile range (IQR) of at least 0.8. A Pearson correlation coefficient was calculated comparing this standard vector to the vector of median centered gene expression for each patient. Patients were classified as positive if the Pearson correlation coefficient was greater than zero, and negative if the coefficient was less than zero. The association between metabolic cluster and wound response score was evaluated using a two-tailed, Fisher's exact test (performed in SAS version 9.2).

Cell culture

Primary CAFs were isolated from breast tissue of patients undergoing breast surgery for primary invasive breast carcinoma at UNC Hospital. Tissue specimens were procured under an IRB-approved protocol (LCC 0913) by the Lineberger Cancer Center Tissue Procurement Facility and stored in 10 mL of DMEM/F12 with 10% FBS on ice until processing (up to 6 hours). Tissue was minced and transferred to a 15 mL conical tube with 9 mL of suspension media: DMEM/F12 (GIBCO) supplemented with 10% FBS (GIBCO), 1% Pen/Strep (Invitrogen), 2.5 ug/mL Amphotericin B solution (Invitrogen), 300 U/mL collagenase (Sigma) and 100 U/ml hyaluronidas (Sigma). Collagenase digestion occurred overnight at 37°C and the sample was then centrifuged for 30 seconds at $100 \times g$. A top layer of hydrolyzed fat was discarded and supernatant was centrifuged at $200 \times g$ for 3 minutes. Supernatant was transferred to a new tube and centrifuged at $400 \times g$ for 5 min. The supernatant was discarded, and the remaining fibroblast pellet was resuspended in 7mL of suspension media, as described above, and transferred to a T25 flask. Cells were grown at 37°C in a 5% CO_2, with media changed every 3-5 days and split into a T75 at 80% confluency.

SUM149 (basal-like) and MCF7 (luminal) breast cancer cell lines were obtained from ATCC (30). Cell lines were maintained 37°C and 5% CO_2 in DMEM/F12 supplemented with 10% FBS and 50 units/mL Penicillin/Streptomycin. Cell lines were tested for mycoplasma by the Tissue Culture Facility at Lineberger Cancer Center.

Cocultures

Two types of cocultures were performed to model the tumor metabolic microenvironment. First, we performed *direct cocultures*, defined as a coculture where the two cell types are grown in physical contact, in the same well. Direct cocultures were used for all of the glucose assays plated at a physiologically relevant 1:2 ratio of cancer cells to fibroblasts in 24-well plates and were maintained for 96 hours, changing the media at 48 hours, before assays were performed. Second, we performed *indirect cocultures* or *transwell cultures*, where fibroblasts and cancer cells are grown separated by a membrane but in contact via soluble factors. Indirect cocultures were solely used to calculate individual cell growth rates for interacting stromal and epithelial cells. These studies were performed by seeding one of the two cell types on the insert layer of Corning Transwell plates with 0.4-mm pore polycarbonate membranes whereas the other cell type was grown in the bottom of the well.

At 96 hours, 48 hours after media change, cells were harvested from top and bottom wells and counted using a Coulter Counter (Beckman Coulter, Inc.) to determine the ratio of cells. Identical starting stromal-epithelial ratios and analysis time points were used for both direct and indirect cultures. Two luminal and one basal-like primary CAF cell lines were used for all *in vitro* experiments and all experiments were repeated in triplicate. For HGF inhibition, cells were treated with 0.5μg/mL of anti-HGF antibody (Abcam) at time of plating, and media was not changed during the course of the experiment (48 hours).

Glucose uptake assay

Cells were plated for direct coculture at 1.0×10^5 epithelial cells/well and 2.0×10^5 fibroblasts/well into 24 well plates and allowed to grow for 96 hours, with media changed at 48 hours. Cells that were treated with anti-HGF antibody or sham were assayed at 48 hours. The cells were washed twice with 0.5 ml 37°C 1× PBS and then incubated for 10 minutes at 37°C in 0.5 ml/well KRH buffer (136 mM NaCl, 4.7 mM KCl, 1.25 mM CaCl₂, 1.25 mM MgSO₄, 10 mM HEPES, pH 7.4) with 0.5 μCi/ml [³H]2-Deoxy-D-glucose (PerkinElmer, Waltham, MA). Cells were washed twice with 0.5 ml iced 1× PBS with 20 mM D-glucose and then lysed in 0.5 ml lysis buffer (0.025% SDS, 1% TX-100 in 1× PBS). Lysates were centrifuged at $20,000 \times g$ for 5 minutes at 4°C and the protein concentration was determined with a Bicinchoninic Acid (BCA) assay (Thermo Fisher Scientific). The rest of the lysate was then added to a scintillation vial filled with 4.5 ml EcoScint H (National Diagnostics, Atlanta, GA) for scintillation counting. Because cell composition changes during the time of coculture (due to different growth rates for cancer cells and fibroblasts), expected metabolic responses for cocultures was computed using cell numbers at time of measurement and using measured activity levels. For each of *n* cocultures, the following formula was used to calculate expected metabolic activity level:

$$m_{n.\text{coculture}} = \left\{ \left(a \cdot m_{\text{epi.mono}} \right) + \left((1-a) \cdot m_{\text{caf.mono}} \right) \right\}$$

Where m = metabolic activity and a = fraction of epithelial cells as estimated by cell counts for both cell types at a given time point after the start of coculture. Expected activity computed by this formula was compared to observed activity, and fold change was computed as a function of expected over observed metabolic activity. Statistical analyses of these data were performed with two-tailed t-tests (e.g. all MCF7 cocultures vs. all SUM149 cocultures, or all LCAF cocultures vs. BCAF cocultures, etc.).

Glucose oxidation/glycogen synthesis

Cells were plated for direct coculture at 1.0×10^5 epithelial cells/well and 2.0×10^5 fibroblasts/well into 24 well plates and allowed to grow for 96 hours, with media changed at 48 hours. The cells were washed twice with 0.5 ml 37°C 1× PBS and then incubated for 120 minutes at 37°C in 0.5 ml/well KRH buffer (136 mM NaCl, 4.7 mM KCl, 1.25 mM CaCl₂, 1.25 mM MgSO₄, 10 mM HEPES, pH 7.4) with 2 μCi/ml [14C] uniformly labeled D-glucose (PerkinElmer). Following incubation, 400 μl of KRH media from each well was placed into the upper well of an oxidation plate with 200 μl 1M NaOH in the lower well. The oxidation plate was sealed with a gasket and lid and the media well acidified by injecting 100 μl 70% perchloric acid. The oxidation plate was placed on an orbital shaker for 1 hour and then 150 μl of the NaOH from each well was placed into a scintillation tube with 4.5 ml EcoScint H for scintillation counting. The data are expressed as DPM/mg of protein/minute. Cells from this assay were washed twice with 0.5 ml iced 1× PBS with 20 mM D-glucose and then lysed in 0.5 ml lysis buffer (30% KOH saturated with Na₂SO₄). Lysates were heated to 95°C for 10 minutes and centrifuged at $20,000 \times g$ for 5 minutes at

4°C. The protein concentration was determined with a BCA assay (Thermo Fisher Scientific). To the remaining lysate, an equal volume of 100% ethanol was added to precipitate glycogen and samples stored at -20°C overnight. Samples were centrifuged at $20,000 \times g$ for 5 minutes at 4°C and the supernatant removed. The pellets were washed in 1 ml of 70% ethanol and centrifuged at $20,000 \times g$ for 5 minutes at 4°C. Supernatants were removed and pellets air-dried overnight. Pellets were then resuspended in 0.5 ml water and transferred to a scintillation vial with 4.5 ml EcoScint H for scintillation counting. The data are expressed as DPM/mg of protein/hr fold change of observed/expected. For each of these cocultures, the expected activity of glucose oxidation and glycogen synthesis pathways were computed as described above and used to compute fold change relative to expected. Statistical analyses of these data were performed as described above for glucose uptake.

Lactate assay

Cells were plated at 1.0×10^5 epithelial cells/well and 2.0×10^5 fibroblasts/well into 24 well plates and allowed to grow for 48 hours, media was collected and stored in aliquots at -80°C and assayed for lactate content. Briefly, fresh NAD+ was added to assay buffer (175 mM Hydrazine Sulfate, 68 mM Glycine, 2.9 mM EDTA, 11.3 mM NAD+, pH 9.5) just prior to assay. In a 96-well plate, 200 μl of assay buffer and 40 μl of lactate standard or media sample were combined in each well. The plate was then pre-read at 340 nm followed by the addition of 1U of lactate dehydrogenase in a 10 μl volume of water. The plate was mixed and read at 340 nm. The lactate concentration in each sample was determined from the standard curve. Computed expected levels of lactate were performed as described for other metabolic assays above. Statistical analyses of these data were performed as described above for glucose uptake.

Western Blot

Cells were harvested from culture and protein was isolated and quantitated. Lysates were denatured by boiling with β-mercaptoethanol and 30μg of protein were electrophoresed on a 4–20% Tris-HCl Criterion precast gel (Bio-Rad) and transferred to a Hybond-P membrane (Amersham Biosciences) by electroblotting. The blots were probed with antibodies against the GLUT1 (Abcam) and β-actin (Cell signaling). Blots were washed three times with Tris-buffered saline supplemented with 0.1% TWEEN and then were probed with ECL anti-mouse IgG horseradish peroxidase-linked whole antibody from rabbit (Amersham-GE Healthscience). Blots were rewashed, and detection was by enhanced chemiluminescence western blotting detection system (Amersham-GE Healthcare). Relative GLUT1 protein concentration was quantified using ImageJ software, pixel intensity was used to measure the protein band of GLUT1 and divided by the intensity of the β-actin band.

Analysis of cytokine expression in conditioned media

Conditioned media from direct 1:1 cocultures (48hours) was analyzed on a RayBio Human Cytokine Antibody Array 5 (80) (Raybiotech) designed to detect 80 cytokines and chemokines. These glass arrays were used according to manufacturer protocol to measure cytokine and chemokine expression in the conditioned media from direct cocultures. Briefly, slides were blocked by incubation with blocking buffer at room temperature for 30 min and incubated with 100 ul of the sample at room temperature for 90min. Membranes were washed and incubated with biotin-conjugated antibodies overnight at 4°C. Finally, the membranes were washed and incubated with fluorescent dye-conjugated streptavidin at room temperature for 2 hours. After final washing, slides were dried by centrifugation at 1000rpm for 3 minutes. Fluorescent signal was detected on a laser scanner using a cy3 (green) channel (excitation frequency 532nm). Data for each cytokine were normalized to positive controls on the same slide to estimate relative protein expression. Each monoculture or direct coculture was analyzed in duplicate.

cDNA Synthesis and qPCR Analysis

RNA was isolated from cultured cells using RNeasy Mini kit (Qiagen) following manufacturers' instructions. 1µg of total RNA was reverse transcribed into cDNA using iScript cDNA synthesis kid (Bio-Rad). qPCR was performed with a dilution of cDNA equivalent to 100ng RNA in 18µl of master mix (10 µl SsoFast 2× Probes Supermix (Bio-Rad), 0.5 µl 18S-VIC and 0.5 µl gene specific Assay-On-Demand-FAM (Applied Biosystems), 7 µl water) was used in each well of the qPCR 96-well plate. The following primer/probe sets (Applied Biosystems) were used: GLUT1, 18S. Amplification conditions were as follows: 1 cycle of 95°C for 1 minute; 40 cycles of 95°C for 5 seconds, 60°C for 20 seconds. The best linear fit equation generated by the amplicon standard curve was used to determine the number of copies of GLUT1 in the cDNA generated. Relative transporter expression was normalized to the expression of 18s. Statistical analyses of these data were performed with a two-tailed t-test (e.g. cocultures vs. monocultures, or cocultures with and without HGF antibody).

Results

Evidence of two distinct metabolic clusters

To identify metabolic subgroups of tumors, unsupervised hierarchical clustering was performed on 379 metabolites across 31 breast tumor and 6 normal breast tissue samples. Patient characteristics for these 37 patients are described in Table 1. Two main clusters resulted (dendrogram shown in Figure 1A and heatmap shown in Figure 1C), one of which (Cluster 1) was primarily normal tissue and less aggressive tumors (90% of luminal A tumors; 100% of normal breast tissues) (Figure 1B, colored boxes). The other cluster (Cluster 2) was enriched for more aggressive tumor subtypes and metastatic tumors (60% of basal-like tumors; 66.7% of luminal B tumors; 100% of metastases). Cluster 2 tumors had significantly larger tumor size (p=0.047) than those in Cluster 1. While associations were not statistically significant, Cluster 2 tumors were also substantially more likely to be ER negative (Figure 1B, gray scale boxes) and have poorly differentiated tumor grade.

Given the importance of stromal cells in altering glucose metabolism of cancer cells in previous literature (10, 31, 32), we hypothesized that metabolite subtypes would correlate with stroma-driven gene expression in the human tissue specimens. Using a published wound response signature identified in cancer-adjacent stroma-rich breast tissue when compared to breast tissue from reduction mammoplasty (25), we observed an association between metabolic cluster and wound response, with a higher percentage of tumors in Cluster 2 (the more aggressive metabolic group) expressing activated wound response signature (Figure 1D, p=0.054). Of the tumors in Cluster 1, 39% were positively correlated with the wound response signature, while 79% of tumors in Cluster 2 were positively correlated with the signature. Interestingly, the association between metabolic subtype and wound response signature was stronger than the association with either ER status or breast tumor subtype (Table 1).

Pathway driven metabolic phenotypes in breast tumors

Four well-defined groups of metabolites defined the differences between metabolic clusters: amino acids, sugars, nucleic acids, and metabolites involved in the tricarboxylic citric acid (TCA) cycle. Principal Component Analysis (PCA) using metabolites in each of these four metabolite classes separated the Cluster 1 and 2 tumors and delineated normal from metastatic samples (Figure 2). The association between metabolite levels and metabolite cluster was strongest for amino acids (Figure 2A, PC1-85.7%, PC2-4.3%), followed by nucleic acids (Figure 2B, PC1-51.6%, PC2-24.3%), TCA cycle (Figure 2C, PC1-54.2%, PC2-17.2%), and carbohydrates/sugars (Figure 2D, PC1-32.8%, PC2-13.6%), suggesting the

relative importance of these types of metabolites in driving clustering and aggressive tumor subtype. Considering individual metabolites in each of these four categories, there were 19 amino acids that increased between normal samples and Cluster 1, and between Cluster 1 and non-metastatic tumors in Cluster 2 (Table 2). Many of these metabolites increased further in metastatic tumors from different sites (skin, lung, liver, or brain). Several individual metabolites showed a trend from normal to Cluster 1 tumors to Cluster 2non-metastatic tumors, including glucose (decrease), glucose-6-phosphate (increase), lactate (increase) and ribulose-5-phosphate (increase). Malic acid and fumaric acid, both metabolites in the TCA cycle, increased from normal to Cluster 1 tumors to Cluster 2 non-metastatic tumors, inversely proportional to citric acid levels. In summary, many metabolites that are crucial for glucose metabolism and the citric acid cycle were present at lower or higher levels in the more aggressive tumor cluster (Cluster 2) compared to Cluster 1. A diagram illustrating the pathways affected by this metabolic shift is presented in Figure 3.

Metabolic processes indicate stroma-influenced Warburg Effect

Previous experimental studies focused on specific metabolic hallmarks of Warburg phenomenon recently identified a 'Reverse Warburg effect', where stromal cells act as important drivers of the metabolic phenotype of cancers (10, 11, 14, 15, 33). Given this previous literature and the correlation between metabolic phenotype and wound response genomic signature, we performed cocultures that modeled basal-like and luminal metabolic microenvironments to assess whether fibroblast characteristics, cancer cell characteristics, or interactions between the two were important in tumor metabolism. Basal-like microenvironments were modeled with SUM149 basal-like breast cancer cells and with basal-like cancer associated fibroblasts (BCAFs). Luminal microenvironments were modeled with MCF7 luminal breast cancer cells and luminal cancer-associated fibroblasts (LCAFs). Results demonstrated a complex interplay of stromal and epithelial cells in determining metabolic phenotype.

Consistent with the observation that more aggressive subtypes have more extreme metabolic phenotypes, SUM149 (basal-like)cells displayed higher glucose uptake than MCF7 (luminal) cells in monoculture (Supplemental Figure 1A). However SUM149 cells had even greater glucose uptake when grown with BCAFs (Figure 4A), showing a 2.9-fold increase in observed relative to expected (p<0.001). BCAFs also increased MCF7 glucose uptake (1.9-fold higher than expected, p=0.001). In contrast, LCAFs suppressed glucose uptake in MCF7 cocultures, but had no effect in coculture withSUM149 cells. Overall, BCAF cocultures had a 2.8 fold increase in glucose uptake when compared to LCAF cocultures (p=0.04).

Once glucose is taken up, utilization includes glucose oxidation, glycogen synthesis, and lactate production, which are endpoints of oxidative metabolism, storage, and glycolysis, respectively. Basal-like cells had higher glucose oxidation in monoculture (Supplemental Figure 1). However, glucose oxidation was suppressed in all luminal coculture conditions (MCF7 cells or LCAFs present, Figure 4B). Increased glucose oxidation among SUM149 cells occurred only when these cells were cocultured with BCAFs (2.1-fold higher glucose oxidation compared to SUM149s with LCAFs, p<0.001). This is interesting, suggesting that both stromal and epithelial factors contribute to glucose oxidation.

Glucose oxidation in the cell is balanced by non-oxidative glucose utilization, including glycogen synthesis. Stored cellular glycogen can promote cell survival in conditions of hypoxia (33). Glycogen synthesis was increased in all cocultures relative to monocultures (Figure 4C), however the increase in glycogen synthesis was most noticeable among SUM149 cocultures.

Finally, we assessed lactate as a measure of anaerobic glycolysis. Lactate production was higher in basal-like cancer cells and cancer-associated fibroblasts than in luminal cells in monoculture (Figure S1A), however all coculture models showed about a 1.5-fold higher than expected lactate production that was not subtype driven (Figure S1B). Considering all of these metabolites, coculture of basal-like epithelial cells with basal-like fibroblasts revealed the strongest phenotype of elevated glucose metabolism including glycolysis, oxidation, and storage.

Glucose uptake regulated by tumor-stromal interactions between GLUT1and HGF

Given the importance of stromal cells in altering glucose metabolism of cancer cells in previous literature (10, 32, 33) and our coculture data, we hypothesized that the expression of glucose transporters may be regulated by tumor-stromal interactions. GLUTs 1-4 are Class I integral membrane proteins responsible for the transport of glucose. We focused on GLUT1 because it is responsible for basal levels of glucose uptake in all cells and glucose levels inversely regulate its expression (34). GLUT1 has also been shown to be the predominant glucose transporter in human breast carcinomas and mouse mammary carcinomas (35, 36). GLUT1 protein levels were higher in the more aggressive SUM149 monocultures when compared to MCF7 monocultures (Figure 5A). Coculture conditions further increased GLUT1 protein levels in both cell types, demonstrating a role for stroma in the regulation of glucose metabolism (Figure 5A). To identify soluble factors and specific pathways regulating this change in GLUT1, cytokine protein arrays were performed. These results indicated significantly higher levels of HGF in coculture conditions (Figure 5B). Consistent with previous data in muscle (37), we hypothesized that HGF was playing a regulatory role in GLUT1 expression. We were able to completely block GLUT1 RNA expression by inhibiting HGF levels in the media, confirming our hypothesis (Figure 5C). To further confirm this mechanism and its downstream effects on metabolism, we compared levels of glucose uptake in stromal-epithelial cocultures with and without HGF inhibition. Our results show 65.6% decrease in glucose uptake (p=0.055) with HGF inhibition in SUM149:RMFcocultures (Figure 5D).

Discussion

Gillies and Gatenby (38) have argued that adaptations to resource scarcity are fundamental in the evolution of carcinogenesis and have shown a variety of pathways dysregulate aerobic glycolysis in tumors (39). Consistent with metabolic adaptation during carcinogenesis, metabolite profiles can distinguish cancer from non-cancer (40). However, while it has been increasingly recognized that cancers evolve into distinct breast cancer subtypes, few studies have evaluated evolution of metabolic differences between breast cancer subtypes (39, 41-44). Our study demonstrates that tumors differ from normal samples in their metabolomic profiles, but extended this to describe metabolomic heterogeneity within tumors. High resolution quantitative profiling of metabolites from normal and tumor tissue identified two metabolic subgroups that were associated with aggressive tumor characteristics. Interestingly, though, these metabolic subtypes did not strongly correlate with established PAM50 or claudin low tumor gene expression subtypes. While larger studies are warranted to allow better powered analysis of how intrinsic subtype affects metabolism, an important next step was to understand whether other genomic signals correlate with metabolic subgroups.

We hypothesized that interactions between tumor epithelium and stroma can be detected in genomic data, and that these interactions contribute to the evolution of distinct metabolic microenvironments. Previous genomic studies have emphasized the importance of host-tumor interactions in progression (45), suggesting possible pathways to test in association with metabolomic subtype. From microarray studies, a wound response is tumor promoting

in the presence of initiated cells (46, 47) and wound response gene signatures are prevalent in tumor adjacent, stroma-enriched tissue (25). Thus, we tested an *in vivo* wound response signature and found its expression to be strongly associated with metabolic subtype. These results demonstrate that integrated analyses of metabolite and gene expression data can identify phenotypically distinct groups of breast cancers.

Other recent papers have performed integrated analyses of metabolomics and gene expression datasets, emphasizing identification of genes associated with individual metabolite levels or identification of metabolic phenotypes associated with specific tumor characteristics (48-51). A large study of metabolite profiles across 289 tumor samples identified groups of tumors corresponding to hormone receptor status and grade, however, that study did not seek to identify associated genomic changes beyond these tumor characteristics (49). Borgan et al. analyzed metabolite profiles of 46 mostly luminal A breast cancers (48) and linked metabolic heterogeneity within the luminal A breast cancers to gene expression differences, including differences in extra cellular matrix (ECM) genes. Their observation of the importance of ECM genes in metabolism is consistent with our finding that metabolism was strongly correlated with stromal signature and stromal-epithelial interactions. Also consistent with our findings, Borgan et al. noted heterogeneity within the luminal A subtype, demonstrating that intrinsic subtype alone does not determine metabolic phenotype (48). In our study, we aimed to include a more diverse sample set with six different subtypes of breast cancer and an approximately even distribution of ER+ and ER- tumors. Our power to perform comprehensive assessments of subtype-specific changes was limited due to sample size, but our results do suggest heterogeneity of response within classes defined by tumor subtype.

Few integrated, observational studies of gene expression and metabolomics data, including our own dataset, have been of sufficient size to evaluate both tumor and stromal characteristics. To address this limitation, we combined our tissue-based observations with well-established cell culture based models that mimic the tumor interactions with microenvironment (5) to confirm the pathway changes seen in our gene expression and metabolomics data. While we were unable to measure all metabolites, we selected the metabolism of glucose for more focused investigation because it is central to many of the Warburg-like changes observed in the full metabolic profile. Our results demonstrate that metabolic phenotype is a complex interplay between tumor characteristics and the surrounding stromal biology. Basal-like breast cancer epithelial cells more readily take up glucose from surrounding tissue than luminal breast cancer cells. Furthermore, basal-like CAFs also stimulate marked increases in glucose uptake, even in luminal breast cancer cells. Conversely, luminal CAFs produce no change or can slightly decrease glucose uptake and oxidation in basal-like breast cancer cells. Glucose oxidation depended on both stromal and epithelial characteristics, while glycogen synthesis appears to be less sensitive to the differences between luminal CAFs and basal-like CAFs, correlating most strongly with epithelial cell content. This latter pattern of metabolite production in coculture suggests an acquired capability – increased glycogen storage in response to micro environmental signals – and raises the question as to whether increased glycogen synthesis is a hallmark of basal-like breast cancers.

While primary CAFs used in this study demonstrate that there is interindividual variation in the effect of CAFs, to establish central trends for basal-like vs. luminal stroma will require greater numbers of cell lines. However, these results underscore the importance of understanding variation in tumor stroma. Characteristics of fibroblasts, such as aging or senescence phenotypes, can also alter metabolism as shown in recent studies (52). Our results confirm that understanding which metabolites are sensitive to stromal factors and

which are dominated by epithelial characteristics is necessary if metabolic processes are to be targeted for cancer treatment or prevention.

Future metabolic-targeted treatment demands understanding of not just the metabolomics phenotypes, but the genomic signals/pathways that drive these phenotypes. We performed cytokine arrays to identify factors induced in coculture that could explain the shift to greater glucose uptake. Having observed large fold changes in HGF secretion, we conducted a literature search that suggested GLUT1 expression is downstream of HGF-cMET signaling in liver and muscle (53, 54). Therefore, we hypothesized that the same pathway may be active in breast cancer. Previous literature shows a role for HGF/cMET in breast cancer aggressiveness. MET receptor protein tyrosine kinase regulates cell motility and invasion (55, 56) and is stimulated by HGF (57, 58). Together, the HGF-MET pathway has been shown to regulate stromal-epithelial interactions in multiple cancers (59-63). In breast cancer, HGF/c-MET signaling promotes tumorigenesis (64), increases metastasis (65, 66), and mediates drug resistance in most aggressive breast cancers (67-69). Our results demonstrate that HGF regulates GLUT1 expression, which in turn regulates glucose uptake. Inhibition of exogenous HGF completely blocks GLUT1 expression and decreased glucose uptake. Given the success of small molecule inhibitors of c-MET in the clinic, the HGF/c-MET pathway may also be a target for the regulation of tumor cell metabolism.

In summary, reciprocal interactions between cancer epithelial cells and the surrounding microenvironment have an established impact on tumor growth (5, 6, 46) and a broad range of other metabolic and signaling processes (26, 43, 70). Previous studies by Lisanti et al. have shown extensive evidence *in vitro* for the stromal role in Warburg metabolism through matrix remodeling (2), stromal autophagy (11), and stromal-epithelial lactate exchange (71). Our results further demonstrate that both fibroblast and epithelial characteristics modulate specific metabolic phenotypes in vitro and pairs one of these changes, glucose uptake, with specific targetable gene expression changes (HGF/GLUT1). This study demonstrates that integration of multiple data types in human tumor studies, together with *in vitro* experimental studies that dissect heterotypic interactions, can yield important advances in understanding the complex metabolic and genomic interactions during tumor evolution.

Supplementary Material

Refer to Web version on PubMed Central for supplementary material.

Acknowledgments

References

1. Garber K. Energy deregulation: licensing tumors to grow. Science. 2006; 312(5777):1158–9. Epub 2006/05/27. [PubMed: 16728625]

2. Castello-Cros R, Bonnucelli G, Molchansky A, Capozza F, Witkiewicz AK, Birbe RC, et al. Matrix remodeling stimulates stromal autophagy, "fueling" cancer cell mitochondrial metabolism and metastasis. Cell Cycle. 2011; 10(12):2021–34. [PubMed: 21646868]

3. Gatenby RA, Gillies RJ. Why do cancers have high aerobic glycolysis? Nature reviews Cancer. 2004; 4(11):891–9. Epub 2004/11/02.

4. Warburg O, Wind F, Negelein E. The Metabolism of Tumors in the Body. The Journal of general physiology. 1927; 8(6):519–30. Epub 1927/03/07. [PubMed: 19872213]

5. Camp JT, Elloumi F, Roman-Perez E, Rein J, Stewart DA, Harrell JC, et al. Interactions with fibroblasts are distinct in Basal-like and luminal breast cancers. Molecular cancer research : MCR. 2011; 9(1):3–13. Epub 2010/12/07. [PubMed: 21131600]

6. De Clerck YA, Weissman BE, Yu D, Parsons R, Bar-Eli M, Roy-Burman P, et al. Tumor progression and metastasis from genetic to microenvironmental determinants: a workshop of the tumor progression and metastasis NIH study section in honor of Dr. Martin L. Padarathsingh, May 31, 2006, Georgetown, Washington, DC. Cancer biology & therapy. 2006; 5(12):1588–99. Epub 2007/01/17. [PubMed: 17224636]

7. Gatza ML, Kung HN, Blackwell KL, Dewhirst MW, Marks JR, Chi JT. Analysis of tumor environmental response and oncogenic pathway activation identifies distinct basal and luminal features in HER2-related breast tumor subtypes. Breast cancer research : BCR. 2011; 13(3):R62. Epub 2011/06/16. [PubMed: 21672245]

8. Tlsty TD, Coussens LM. Tumor stroma and regulation of cancer development. Annual review of pathology. 2006; 1:119–50. Epub 2007/11/28.

9. Martinez-Outschoorn UE, Balliet RM, Rivadeneira DB, Chiavarina B, Pavlides S, Wang C, et al. Oxidative stress in cancer associated fibroblasts drives tumor-stroma co-evolution: A new paradigm for understanding tumor metabolism, the field effect and genomic instability in cancer cells. Cell Cycle. 2010; 9(16):3256–76. Epub 2010/09/04. [PubMed: 20814239]

10. Martinez-Outschoorn UE, Pavlides S, Howell A, Pestell RG, Tanowitz HB, Sotgia F, et al. Stromal-epithelial metabolic coupling in cancer: integrating autophagy and metabolism in the tumor microenvironment. The international journal of biochemistry & cell biology. 2011; 43(7): 1045–51. Epub 2011/02/09.

11. Martinez-Outschoorn UE, Trimmer C, Lin Z, Whitaker-Menezes D, Chiavarina B, Zhou J, et al. Autophagy in cancer associated fibroblasts promotes tumor cell survival: Role of hypoxia, HIF1 induction and NFkappaB activation in the tumor stromal microenvironment. Cell Cycle. 2010; 9(17):3515–33. Epub 2010/09/22. [PubMed: 20855962]

12. Stewart DA, Yang Y, Makowski L, Troester MA. Basal-like Breast Cancer Cells Induce Phenotypic and Genomic Changes in Macrophages. Molecular cancer research : MCR. 2012; 10(6):727–38. Epub 2012/04/26. [PubMed: 22532586]

13. Martinez-Outschoorn UE, Lin Z, Trimmer C, Flomenberg N, Wang C, Pavlides S, et al. Cancer cells metabolically "fertilize" the tumor microenvironment with hydrogen peroxide, driving the Warburg effect: Implications for PET imaging of human tumors. Cell Cycle. 2011; 10(15):2504–20. [PubMed: 21778829]

14. Pavlides S, Whitaker-Menezes D, Castello-Cros R, Flomenberg N, Witkiewicz AK, Frank PG, et al. The reverse Warburg effect: aerobic glycolysis in cancer associated fibroblasts and the tumor stroma. Cell Cycle. 2009; 8(23):3984–4001. Epub 2009/11/20. [PubMed: 19923890]

15. Pavlides S, Tsirigos A, Vera I, Flomenberg N, Frank PG, Casimiro MC, et al. Transcriptional evidence for the "Reverse Warburg Effect" in human breast cancer tumor stroma and metastasis: similarities with oxidative stress, inflammation, Alzheimer's disease, and "Neuron-Glia Metabolic Coupling". Aging. 2010; 2(4):185–99. Epub 2010/05/06. [PubMed: 20442453]

16. Pavlides S, Tsirigos A, Migneco G, Whitaker-Menezes D, Chiavarina B, Flomenberg N, et al. The autophagic tumor stroma model of cancer: Role of oxidative stress and ketone production in fueling tumor cell metabolism. Cell Cycle. 2010; 9(17):3485–505. Epub 2010/09/24. [PubMed: 20861672]

17. Perou CM, Sorlie T, Eisen MB, van de Rijn M, Jeffrey SS, Rees CA, et al. Molecular portraits of human breast tumours. Nature. 2000; 406(6797):747–52. Epub 2000/08/30. [PubMed: 10963602]

18. Fan C, Prat A, Parker JS, Liu Y, Carey LA, Troester MA, et al. Building prognostic models for breast cancer patients using clinical variables and hundreds of gene expression signatures. BMC medical genomics. 2011; 4:3. Epub 2011/01/11. [PubMed: 21214954]

19. Ross DT, Perou CM. A comparison of gene expression signatures from breast tumors and breast tissue derived cell lines. Disease markers. 2001; 17(2):99–109. Epub 2001/10/24. [PubMed: 11673656]

20. Prat A, Parker JS, Karginova O, Fan C, Livasy C, Herschkowitz JI, et al. Phenotypic and molecular characterization of the claudin-low intrinsic subtype of breast cancer. Breast cancer research : BCR. 2010; 12(5):R68. Epub 2010/09/04. [PubMed: 20813035]

21. Santarpia L, Qi Y, Stemke-Hale K, Wang B, Young EJ, Booser DJ, et al. Mutation profiling identifies numerous rare drug targets and distinct mutation patterns in different clinical subtypes of breast cancers. Breast cancer research and treatment. 2012 Epub 2012/04/28.

22. Rouzier R, Perou CM, Symmans WF, Ibrahim N, Cristofanilli M, Anderson K, et al. Breast cancer molecular subtypes respond differently to preoperative chemotherapy. Clinical cancer research : an official journal of the American Association for Cancer Research. 2005; 11(16):5678–85. Epub 2005/08/24. [PubMed: 16115903]

23. Perou CM, Borresen-Dale AL. Systems biology and genomics of breast cancer. Cold Spring Harbor perspectives in biology. 2011; 3(2) Epub 2010/11/05.

24. Radisky D, Hagios C, Bissell MJ. Tumors are unique organs defined by abnormal signaling and context. Seminars in cancer biology. 2001; 11(2):87–95. Epub 2001/04/27. [PubMed: 11322828]

25. Troester MA, Lee MH, Carter M, Fan C, Cowan DW, Perez ER, et al. Activation of host wound responses in breast cancer microenvironment. Clinical cancer research : an official journal of the American Association for Cancer Research. 2009; 15(22):7020–8. Epub 2009/11/06. [PubMed: 19887484]

26. Hu Z, Fan C, Oh DS, Marron JS, He X, Qaqish BF, et al. The molecular portraits of breast tumors are conserved across microarray platforms. BMC genomics. 2006; 7:96. Epub 2006/04/29. [PubMed: 16643655]

27. Tusher VG, Tibshirani R, Chu G. Significance analysis of microarrays applied to the ionizing radiation response. Proceedings of the National Academy of Sciences of the United States of America. 2001; 98(9):5116–21. Epub 2001/04/20. [PubMed: 11309499]

28. Page, RD. Visualizing phylogenetic trees using TreeView. Baxevanis, Andreas D., et al., editors. Vol. Chapter 6. Current protocols in bioinformatics/editoral board; 2002. Unit 6 2. Epub 2008/09/17

29. Creighton CJ, Nagaraja AK, Hanash SM, Matzuk MM, Gunaratne PH. A bioinformatics tool for linking gene expression profiling results with public databases of microRNA target predictions. RNA. 2008; 14(11):2290–6. Epub 2008/09/25. [PubMed: 18812437]

30. Neve RM, Chin K, Fridlyand J, Yeh J, Baehner FL, Fevr T, et al. A collection of breast cancer cell lines for the study of functionally distinct cancer subtypes. Cancer cell. 2006; 10(6):515–27. Epub 2006/12/13. [PubMed: 17157791]

31. Pelletier J, Bellot G, Gounon P, Lacas-Gervais S, Pouyssegur J, Mazure NM. Glycogen Synthesis is Induced in Hypoxia by the Hypoxia-Inducible Factor and Promotes Cancer Cell Survival. Frontiers in oncology. 2012; 2:18. Epub 2012/06/01. [PubMed: 22649778]

32. Bonuccelli G, Whitaker-Menezes D, Castello-Cros R, Pavlides S, Pestell RG, Fatatis A, et al. The reverse Warburg effect: glycolysis inhibitors prevent the tumor promoting effects of caveolin-1 deficient cancer associated fibroblasts. Cell Cycle. 2010; 9(10):1960–71. Epub 2010/05/25. [PubMed: 20495363]

33. Pavlides S, Vera I, Gandara R, Sneddon S, Pestell RG, Mercier I, et al. Warburg Meets Autophagy: Cancer-Associated Fibroblasts Accelerate Tumor Growth and Metastasis via Oxidative Stress, Mitophagy, and Aerobic Glycolysis. Antioxidants & redox signaling. 2011 Epub 2011/09/03.

34. Zhao FQ, Keating AF. Functional properties and genomics of glucose transporters. Current genomics. 2007; 8(2):113–28. Epub 2008/07/29. [PubMed: 18660845]

35. Kang SS, Chun YK, Hur MH, Lee HK, Kim YJ, Hong SR, et al. Clinical significance of glucose transporter 1 (GLUT1) expression in human breast carcinoma. Japanese journal of cancer research : Gann. 2002; 93(10):1123–8. Epub 2002/11/06. [PubMed: 12417042]

36. Young CD, Lewis AS, Rudolph MC, Ruehle MD, Jackman MR, Yun UJ, et al. Modulation of glucose transporter 1 (GLUT1) expression levels alters mouse mammary tumor cell growth in vitro and in vivo. PloS one. 2011; 6(8):e23205. Epub 2011/08/10. [PubMed: 21826239]

37. Perdomo G, Martinez-Brocca MA, Bhatt BA, Brown NF, O'Doherty RM, Garcia-Ocana A. Hepatocyte growth factor is a novel stimulator of glucose uptake and metabolism in skeletal

muscle cells. The Journal of biological chemistry. 2008; 283(20):13700–6. Epub 2008/03/26. [PubMed: 18362143]

38. Gillies RJ, Gatenby RA. Hypoxia and adaptive landscapes in the evolution of carcinogenesis. Cancer metastasis reviews. 2007; 26(2):311–7. Epub 2007/04/04. [PubMed: 17404691]

39. Robey IF, Stephen RM, Brown KS, Baggett BK, Gatenby RA, Gillies RJ. Regulation of the Warburg effect in early-passage breast cancer cells. Neoplasia. 2008; 10(8):745–56. Epub 2008/08/02. [PubMed: 18670636]

40. Wang H, Tso VK, Slupsky CM, Fedorak RN. Metabolomics and detection of colorectal cancer in humans: a systematic review. Future Oncol. 2010; 6(9):1395–406. Epub 2010/10/06. [PubMed: 20919825]

41. Sitter B, Lundgren S, Bathen TF, Halgunset J, Fjosne HE, Gribbestad IS. Comparison of HR MAS MR spectroscopic profiles of breast cancer tissue with clinical parameters. NMR in biomedicine. 2006; 19(1):30–40. Epub 2005/10/18. [PubMed: 16229059]

42. Oakman C, Tenori L, Biganzoli L, Santarpia L, Cappadona S, Luchinat C, et al. Uncovering the metabolomic fingerprint of breast cancer. The international journal of biochemistry & cell biology. 2011; 43(7):1010–20. Epub 2010/05/13.

43. Lisanti MP, Martinez-Outschoorn UE, Chiavarina B, Pavlides S, Whitaker-Menezes D, Tsirigos A, et al. Understanding the "lethal" drivers of tumor-stroma co-evolution: emerging role(s) for hypoxia, oxidative stress and autophagy/mitophagy in the tumor micro-environment. Cancer biology & therapy. 2010; 10(6):537–42. Epub 2010/09/24. [PubMed: 20861671]

44. Brockmoller SF, Bucher E, Muller BM, Budczies J, Hilvo M, Griffin JL, et al. Integration of metabolomics and expression of glycerol-3-phosphate acyltransferase (GPAM) in breast cancer-link to patient survival, hormone receptor status, and metabolic profiling. Journal of proteome research. 2012; 11(2):850–60. Epub 2011/11/11. [PubMed: 22070544]

45. Bissell MJ, Hines WC. Why don't we get more cancer? A proposed role of the microenvironment in restraining cancer progression. Nature medicine. 2011; 17(3):320–9. Epub 2011/03/09.

46. Bissell MJ, Radisky D. Putting tumours in context. Nature reviews Cancer. 2001; 1(1):46–54. Epub 2002/03/20.

47. Sieweke MH, Thompson NL, Sporn MB, Bissell MJ. Mediation of wound-related Rous sarcoma virus tumorigenesis by TGF-beta. Science. 1990; 248(4963):1656–60. Epub 1990/06/29. [PubMed: 2163544]

48. Borgan E, Sitter B, Lingjaerde OC, Johnsen H, Lundgren S, Bathen TF, et al. Merging transcriptomics and metabolomics--advances in breast cancer profiling. BMC cancer. 2010; 10:628. Epub 2010/11/18. [PubMed: 21080935]

49. Denkert C, Bucher E, Hilvo M, Salek R, Oresic M, Griffin J, et al. Metabolomics of human breast cancer: new approaches for tumor typing and biomarker discovery. Genome medicine. 2012; 4(4):37. Epub 2012/05/02. [PubMed: 22546809]

50. Giskeodegard GF, Lundgren S, Sitter B, Fjosne HE, Postma G, Buydens LM, et al. Lactate and glycine-potential MR biomarkers of prognosis in estrogen receptor-positive breast cancers. NMR in biomedicine. 2012 Epub 2012/03/13.

51. Ferrara CT, Wang P, Neto EC, Stevens RD, Bain JR, Wenner BR, et al. Genetic networks of liver metabolism revealed by integration of metabolic and transcriptional profiling. PLoS genetics. 2008; 4(3):e1000034. Epub 2008/03/29. [PubMed: 18369453]

52. Capparelli C, Guido C, Whitaker-Menezes D, Bonuccelli G, Balliet R, Pestell TG, et al. Autophagy and senescence in cancer-associated fibroblasts metabolically supports tumor growth and metastasis via glycolysis and ketone production. Cell Cycle. 2012; 11(12):2285–302. Epub 2012/06/12. [PubMed: 22684298]

53. Bhargava M, Joseph A, Knesel J, Halaban R, Li Y, Pang S, et al. Scatter factor and hepatocyte growth factor: activities, properties, and mechanism. Cell growth & differentiation : the molecular biology journal of the American Association for Cancer Research. 1992; 3(1):11–20. Epub 1992/01/01.

54. Taher TE, Derksen PW, de Boer OJ, Spaargaren M, Teeling P, van der Wal AC, et al. Hepatocyte growth factor triggers signaling cascades mediating vascular smooth muscle cell migration.

Biochemical and biophysical research communications. 2002; 298(1):80–6. Epub 2002/10/16. [PubMed: 12379223]

55. Birchmeier C, Birchmeier W, Gherardi E, Vande Woude GF. Met, metastasis, motility and more. Nature reviews Molecular cell biology. 2003; 4(12):915–25. Epub 2003/12/20.

56. Trusolino L, Bertotti A, Comoglio PM. MET signalling: principles and functions in development, organ regeneration and cancer. Nature reviews Molecular cell biology. 2010; 11(12):834–48. Epub 2010/11/26.

57. Naldini L, Vigna E, Narsimhan RP, Gaudino G, Zarnegar R, Michalopoulos GK, et al. Hepatocyte growth factor (HGF) stimulates the tyrosine kinase activity of the receptor encoded by the proto-oncogene c-MET. Oncogene. 1991; 6(4):501–4. Epub 1991/04/01. [PubMed: 1827664]

58. Weidner, KM.; Arakaki, N.; Hartmann, G.; Vandekerckhove, J.; Weingart, S.; Rieder, H., et al. Evidence for the identity of human scatter factor and human hepatocyte growth factor. Proceedings of the National Academy of Sciences of the United States of America; 1991; p. 7001-5.Epub 1991/08/15

59. Previdi S, Maroni P, Matteucci E, Broggini M, Bendinelli P, Desiderio MA. Interaction between human-breast cancer metastasis and bone microenvironment through activated hepatocyte growth factor/Met and beta-catenin/Wnt pathways. Eur J Cancer. 2010; 46(9):1679–91. Epub 2010/03/31. [PubMed: 20350802]

60. Gos M, Miloszewska J, Przybyszewska M. Epithelial-mesenchymal transition in cancer progression. Postepy biochemii. 2009; 55(2):121–8. Epub 2009/10/15. Rola przejscia epitelialno-mezenchymalnego w progresji nowotworu. [PubMed: 19824467]

61. Lam MM, Swanson PE, Upton MP, Yeh MM. Ovarian-type stroma in hepatobiliary cystadenomas and pancreatic mucinous cystic neoplasms: an immunohistochemical study. American journal of clinical pathology. 2008; 129(2):211–8. Epub 2008/01/23. [PubMed: 18208800]

62. Felix AS, Edwards RP, Stone RA, Chivukula M, Parwani AV, Bowser R, et al. Associations between hepatocyte growth factor, c-Met, and basic fibroblast growth factor and survival in endometrial cancer patients. British journal of cancer. 2012; 106(12):2004–9. Epub 2012/05/24. [PubMed: 22617129]

63. Straussman R, Morikawa T, Shee K, Barzily-Rokni M, Qian ZR, Du J, et al. Tumour micro-environment elicits innate resistance to RAF inhibitors through HGF secretion. Nature. 2012; 487(7408):500–4. Epub 2012/07/06. [PubMed: 22763439]

64. Cheng N, Chytil A, Shyr Y, Joly A, Moses HL. Enhanced hepatocyte growth factor signaling by type II transforming growth factor-beta receptor knockout fibroblasts promotes mammary tumorigenesis. Cancer research. 2007; 67(10):4869–77. Epub 2007/05/15. [PubMed: 17495323]

65. Hwang CI, Choi J, Zhou Z, Flesken-Nikitin A, Tarakhovsky A, Nikitin AY. MET-dependent cancer invasion may be preprogrammed by early alterations of p53-regulated feedforward loop and triggered by stromal cell-derived HGF. Cell Cycle. 2011; 10(22):3834–40. Epub 2011/11/11. [PubMed: 22071625]

66. Shojaei F, Simmons BH, Lee JH, Lappin PB, Christensen JG. HGF/c-Met pathway is one of the mediators of sunitinib-induced tumor cell type-dependent metastasis. Cancer letters. 2012; 320(1): 48–55. Epub 2012/01/25. [PubMed: 22269210]

67. Gastaldi S, Comoglio PM, Trusolino L. The Met oncogene and basal-like breast cancer: another culprit to watch out for? Breast cancer research : BCR. 2010; 12(4):208. Epub 2010/09/02. [PubMed: 20804567]

68. Mueller KL, Madden JM, Zoratti GL, Kuperwasser C, List K, Boerner JL. Fibroblast-secreted hepatocyte growth factor mediates epidermal growth factor receptor tyrosine kinase inhibitor resistance in triple-negative breast cancers through paracrine activation of Met. Breast cancer research : BCR. 2012; 14(4):R104. Epub 2012/07/14. [PubMed: 22788954]

69. Yasui T, Ohuchida K, Zhao M, Onimaru M, Egami T, Fujita H, et al. Tumor-stroma interactions reduce the efficacy of adenoviral therapy through the HGF-MET pathway. Cancer science. 2011; 102(2):484–91. Epub 2010/11/26. [PubMed: 21105966]

70. Potenta S, Zeisberg E, Kalluri R. The role of endothelial-to-mesenchymal transition in cancer progression. British journal of cancer. 2008; 99(9):1375–9. Epub 2008/09/18. [PubMed: 18797460]

71. Whitaker-Menezes D, Martinez-Outschoorn UE, Lin Z, Ertel A, Flomenberg N, Witkiewicz AK, et al. Evidence for a stromal-epithelial "lactate shuttle" in human tumors: MCT4 is a marker of oxidative stress in cancer-associated fibroblasts. Cell Cycle. 2011; 10(11):1772–83. [PubMed: 21558814]

Translational Relevance

Evolutionary theories of cancer argue that tumors must adapt to their local microenvironments to progress, including adaptation to limited oxygen and nutrients. While evolution of breast cancers appears to result in distinct genomic subtypes, the corresponding metabolomic subtypes have not been well characterized. We provide evidence that metabolomic characteristics of tumors are a result of complex interactions between stromal and cancer cells, with stroma-epithelial interactions playing a critical role in substrate metabolism observed in tumors. More aggressive cancers possess a distinct metabolic phenotype, which is weakly associated with cancer subtype, and more strongly associated with expression of a stroma-derived wound response signature. Several studies have suggested that metabolic phenotypes of tumors may be targetable to inhibit tumor growth, but an understanding of the genomic controls upon tissue metabolism is needed. We demonstrate that glucose uptake in epithelial cells, occurs partially through GLUT1 receptor. Epithelial GLUT1 expression, in turn, is dependent upon coculture-derived HGF secretion. Because HGF/c-MET pathway is implicated in other malignancies and c-MET inhibitors are already clinically available, blocking c-MET response to HGF may be a plausible strategy for targeting tumor metabolism.
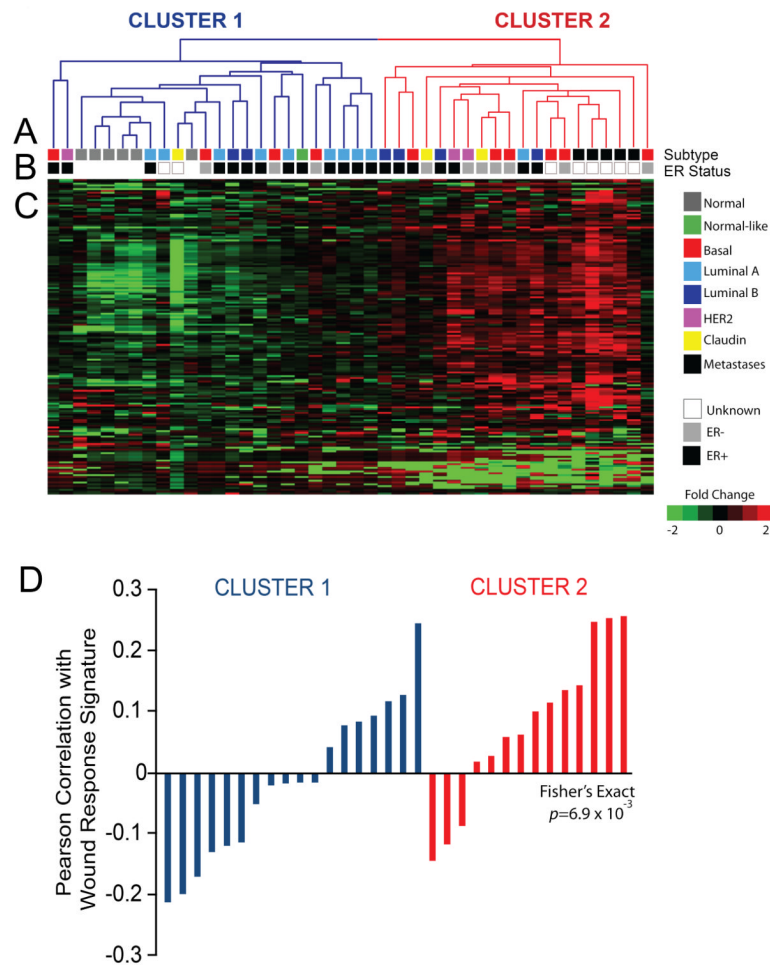
Figure 1. Unsupervised cluster analysis of 379 metabolites resulted in two main clusters (Clusters 1 and 2)

(A). Cluster 1 (blue lines in dendrogram) included less aggressive tumor types or normal breast samples, while Cluster 2 (red lines in dendrogram) included more aggressive tumors and metastases (B, colored bars). Clusters of metabolites in the heatmap (C) implicated hallmark Warburg phenotypes in aggressive tumors: elevated levels of amino acids, nucleic acids, and decreased steady state levels of sugars/carbohydrates and citric acid cycle metabolites. Pearson correlation of tumor gene expression with a previously published wound response signature shows a role for stromal activation in Cluster 2; that is, metabolic class was strongly correlated with expression of an in vivo wound response signature (25) (D).
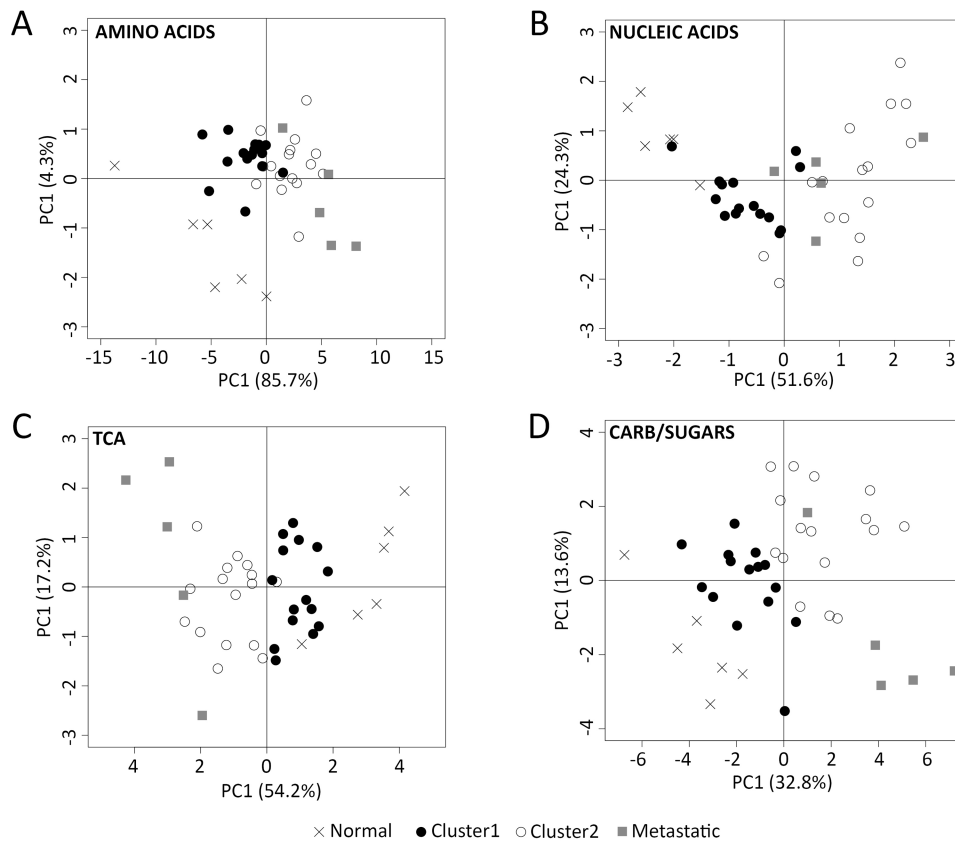
Figure 2. Principal Component Analysis reveals a separation of tumor phenotype by key metabolite groups

Four classes of metabolites – (A) amino acids, (B) nucleic acids, (C) tricarboxylic acid (TCA) cyclemetabolites, and (D)carbohydrates/sugars – distinguish normal breast tissue samples, tumors in the less aggressive metabolite cluster (Cluster 1), tumors in the more aggressive metabolite cluster (Cluster 2), and metastatic tumors.
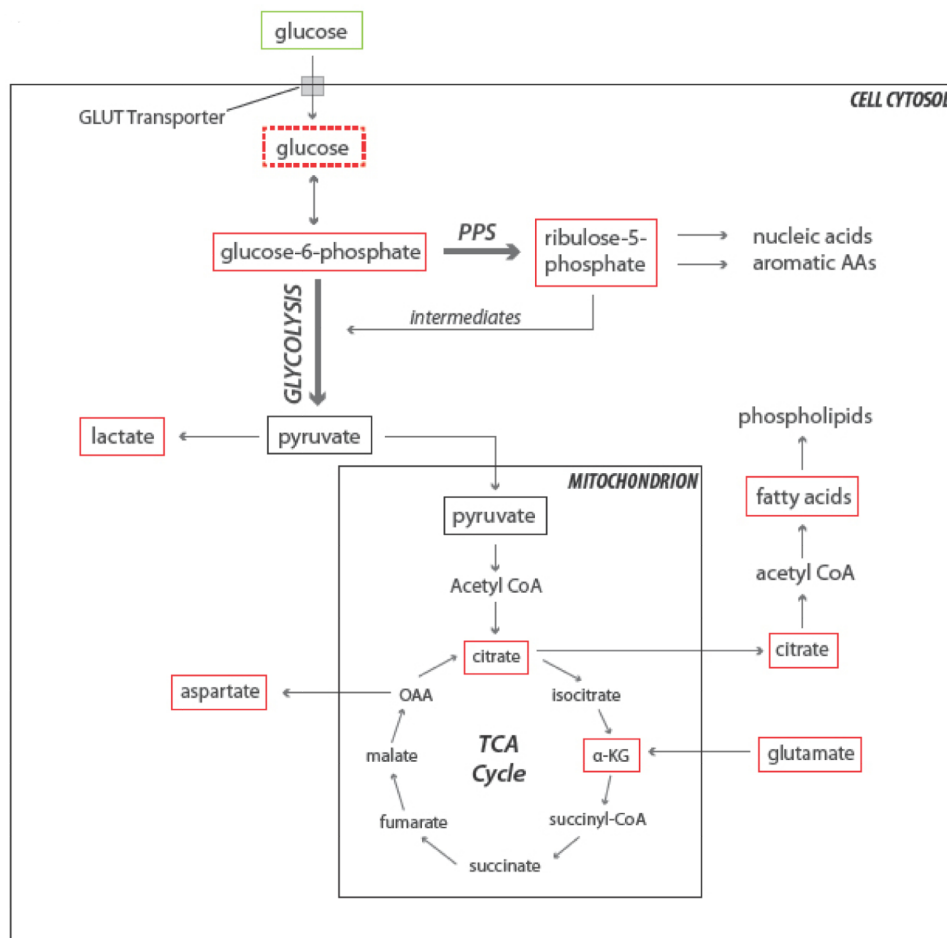
Figure 3. Schematic representing major metabolic pathways in the Warburg effect and their relative levels in distinct groups of breast tumors
Red boxes indicate an increase in metabolite levels in Cluster 2 compared to the less aggressive Cluster 1, while a green box indicates decreasing levels. The dotted red box indicates marginally increased metabolite levels. Glucose processing through glycolysis to pyruvate and lactate provides ATP, while the pentose phosphate shunt (PPS) generates key intermediates in nucleotide biosynthesis. Glucose-derived citrate is exported to the cytosol to contribute to lipid production. Glutamine is converted into glutamate and is transported to the mitochondria where it is de-aminated to generate α-ketoglutarate, an intermediate in the TCA cycle. Aromatic amino acids (Aromatic AAs); oxaloacetate (OAA); Acetyl coenzyme A (Acetyl CoA); Succinyl coenzyme A (Succinyl CoA).
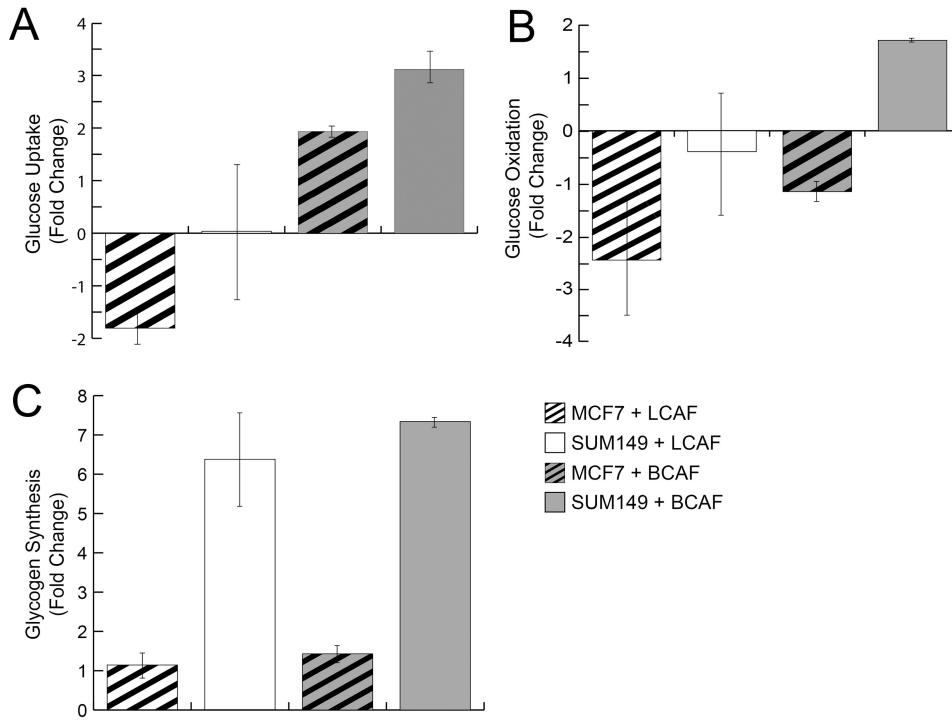
Figure 4. Glucose metabolism is regulated by aggressiveness of both tumor and stroma
Glucose uptake is increased by basal-like CAFs (BCAFs). SUM149 cells had higher levels of glucose uptake than MCF7 cells in coculture regardless of fibroblast type (A). Glucose oxidation was suppressed in luminal cocultures (MCF7 or LCAF), while SUM149 cells cocultured with BCAFs had increased glucose oxidation (B). Finally, analysis of glycogen synthesis (C) revealed an increase in all coculture conditions relative to monocultures, with the strongest fold change among basal-like breast cancer cells (SUM149). All fold change values are expressed relative to the expected levels based on coculture composition and monoculture metabolism, as described in Methods.
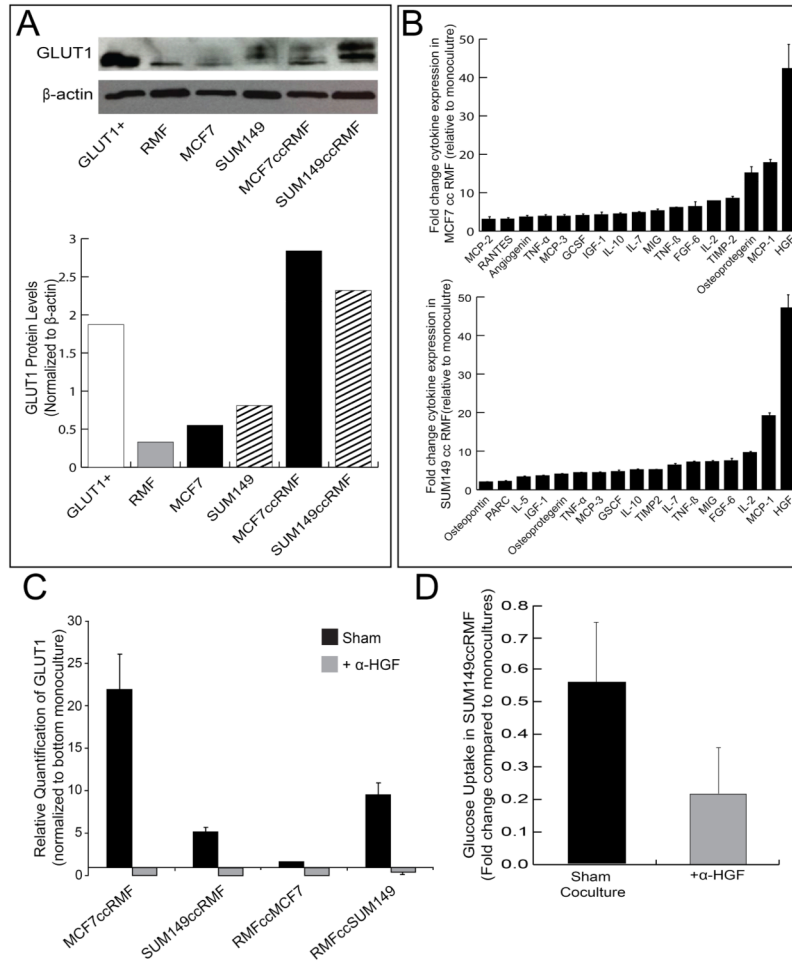
Figure 5. HGF-dependent regulation of GLUT1 expression in breast cancer
HGF protein expression is elevated in coculture (cc) models compared to monocultures of RMF, MCF7 and SUM149 cells(A). Cytokine arrays identify HGF as a key factor significantly induced in coculture for both luminal and basal-like breast cancer cells (B), when blocked using an HGF neutralizing antibody (α-HGF), the GLUT1 receptor is inhibited at the RNA level (C). Levels of glucose uptake decrease by 66% (p=0.055) in SUM149 cells when HGF is inhibited using antibody (D).

Table 1

Characteristics of breast cancer samples by two clusters according to metabolite expression

	Total	Cluster 1 – good prognosis (N=18)		Cluster 2 – poor prognosis (N=15)		
	N	N	%	N	%	p value
ER status						
Positive	20	13	61.1	7	38.9	0.122
Negative	10	3	41.7	7	58.3	
Missing	3	2	66.7	1	33.3	
Size						
<= 2 cm	7	7	100	0	0	
< 2 cm to <= 5cm	12	5	41.7	7	58.3	
< 5cm	5	2	40	3	60	0.047
Direct extension to chest wall or skin	7	3	42.9	4	57.1	
Missing	2	1	50	1	50	
Tumor subtype§						
Basal	10	4	40	6	60	
HER2	3	1	66.7	2	33.3	
Luminal A	10	9	90	1	10	0.064
Luminal B	6	2	33.3	4	66.7	
Claudin-low	3	1	33.3	2	66.7	
Normal-like	1	1	100	0	0	
Tumor Grade						
Well differentiated/1	2	2	100	0	0	
Intermediate/2	7	5	71.4	2	28.6	0.135
Poorly differentiated/3	20	8	40	12	60	
Missing	4	3	75	1	25	
Node#						
Negative	21	12	57.1	9	42.9	
Positive	10	5	50	5	50	0.991
Unknown	2	1	50	1	50	
Age						

	Total	Cluster 1 – good prognosis (N=18)		Cluster 2 – poor prognosis (N=15)		
	N	N	%	N	%	p value
30-39	5	2	40	3	60	
40-49	5	3	60	2	40	
50-59	5	3	60	2	40	0.952
<= 60	16	9	56.3	7	43.7	
Unknown	2	1	50	1	50	

§Classified using PAM50 algorithm applied to microarray data.

#Negative means no positive lymph nodes. Positive is at least one positive lymph node.

Table 2

Mean metabolite levels and trend for four key groups.

| Metabolite§ | Mean Value | | | | β-value (SE)* | P trend** |
	Normal	Cluster 1	Cluster 2	Mets		
Amino Acids						
Alanine	22.2	23.3	24.9	26.1	1.36 (0.12)	<0.001
Proline	21.4	22.7	24.2	25.3	1.36 (0.15)	<0.001
Glycine	21.8	23.8	25.5	26.7	1.67 (0.16)	<0.001
Histidine	18.7	20.0	21.4	22.3	1.27 (0.16)	<0.001
Leucine	21.4	22.5	23.8	24.8	1.18 (0.15)	<0.001
Isoleucine	20.3	20.9	22.3	23.2	1.04 (0.17)	<0.001
Valine	21.0	21.9	23.1	24.0	1.05 (0.14)	<0.001
Threonine	19.4	20.6	22.0	23.1	1.30 (0.16)	<0.001
Methionine	20.3	21.1	22.4	23.1	1.00 (0.14)	<0.001
Serine	20.4	21.7	23.0	23.7	1.18 (0.15)	<0.001
Phenylalanine	22.9	23.4	24.5	25.1	0.82 (0.13)	<0.001
Tyrosine	21.8	22.5	23.6	24.3	0.88 (0.13)	<0.001
Lysine	19.0	20.2	21.0	21.7	0.90 (0.13)	<0.001
Tryptophan	21.4	21.9	22.9	23.8	0.83 (0.13)	<0.001
Arginine	18.4	19.1	19.8	20.4	0.68 (0.13)	<0.001
Asparagine	17.2	18.8	19.6	20.3	0.97 (0.15)	<0.001
Glutamine	20.8	21.7	22.5	23.5	0.87 (0.17)	<0.001
Taurine	16.2	18.7	19.2	19.1	0.90 (0.15)	<0.001
Ornithine	17.0	17.3	17.8	20.0	0.86 (0.18)	<0.001
Carbohydrates/Sugars						
Lactate	23.7	25.4	27.0	27.9	1.49 (0.15)	<0.001
Mannose-6-phosphate	14.4	15.4	17.4	17.8	1.34 (0.18)	<0.001
N-acetylglucosamine 6-phosphate	14.8	15.5	16.9	17.3	0.95 (0.13)	<0.001
Isobar: ribulose 5-phosphate, xylulose 5-phosphate	15.2	15.4	16.9	16.7	0.76 (0.19)	<0.001
Fructose-6-phosphate	15.1	16.6	18.2	18.7	1.31 (0.17)	<0.001

Metabolite§	Mean Value				β-value (SE)*	P trend**
	Normal	Cluster 1	Cluster 2	Mets		
N-acetylneuraminate	15.8	16.2	17.5	18.5	0.98 (0.16)	<0.001
Glucose-6-phosphate	15.9	18.2	19.9	20.5	1.58 (0.21)	<0.001
Erythronate	14.5	15.4	16.8	18.8	1.43 (0.19)	<0.001
UDP-N-acetylgalactosamine	16.0	18.9	20.9	21.3	1.87 (0.30)	<0.001
Glucose	22.4	20.8	19.5	20.5	-0.84 (0.27)	0.004
Glycerate	15.8	15.9	16.4	17.4	0.51 (0.11)	<0.001
Xylitol	17.6	17.8	16.9	18.1	-0.11 (0.19)	0.564
Sedoheptulose-7-phosphate	14.1	13.2	14.2	14.1	0.23 (0.21)	0.273
Maltose	16.7	17.0	17.9	19.4	0.87 (0.23)	<0.001
1,5-anhydroglucitol	17.7	17.7	18.5	18.7	0.41 (0.20)	0.040
Sorbitol	16.8	18.0	17.3	19.0	0.38 (0.23)	0.099
Fructose	17.6	16.2	16.6	18.6	0.29 (0.22)	0.204
3-phosphoglycerate	16.2	16.7	17.2	18.0	0.57 (0.18)	0.004
Mannose	16.8	17.1	16.7	18.1	0.20 (0.19)	0.309
Mannitol	17.6	18.5	18.7	20.9	0.85 (0.27)	0.003
N-acetylmannosamine	17.1	18.0	17.9	17.6	0.13 (0.19)	0.485
Pyruvate	17.3	18.0	17.9	16.6	-0.15 (0.17)	0.391
Phosphoenolpyruvate	15.5	15.3	15.3	15.8	0.13 (0.13)	0.636
Nucleic Acids						
Uracil	14.9	18.1	20.2	21.5	2.21 (0.20)	<0.001
Guanine	15.4	18.2	20.3	18.3	1.32 (0.28)	<0.001
Adenine	17.6	17.6	16.0	16.6	-0.64 (0.23)	0.010
Thymine	17.6	18.0	17.1	16.9	-0.38 (0.20)	0.059
TCA Cycle						
Phosphate	24.2	25.6	27.1	28.1	1.35 (0.10)	<0.001
Fumarate	15.3	16.9	18.8	19.1	1.44 (0.14)	<0.001
Malate	16.4	18.5	20.5	21.0	1.66 (0.17)	<0.001
Alpha-ketoglutarate	13.9	14.0	14.7	19.7	1.56 (0.26)	<0.001

Metabolite[§]	Mean Value				β-value (SE)[*]	P trend[**]
	Normal	Cluster 1	Cluster 2	Mets		
Citrate	18.6	17.9	17.4	17.8	-0.35 (0.19)	0.082
Pyrophosphate (PPi)	18.9	19.9	20.1	20.4	0.47 (0.11)	<0.001
Succinate	15.7	15.8	16.1	18.0	0.016 (0.25)	0.016

[§]Data are reported as mean normalized median centered metabolite levels

[*]β-value (Standard Error) corresponding to linear regression of metabolite level on an ordinal variable equal to 1 for normal, 2 for Cluster 1, 3 for Cluster 2, and 4 for metastases.

[**]P trend column indicates statistical significance of the β-value.